PERGAMON

International Journal of Solids and Structures 36 (1999) 4367–4396

INTERNATIONAL JOURNAL OF SOLIDS and STRUCTURES

Biaxial crushing of honeycombs—Part I: Experiments

S.D. Papka, S. Kyriakides*

Center for Mechanics of Solids, Structures and Materials, The University of Texas at Austin, WRW 110, Austin, TX 78712, U.S.A.

Received 26 February 1998; in revised form 4 July 1998

Abstract

The in-plane compression and crushing of honeycombs is known to be closely related to the crushing behavior of the broader class of space filling cellular solids. Previously, the authors conducted an extensive study of uniaxial crushing of a polycarbonate honeycomb with circular cells. In this paper the same honeycomb is crushed biaxially. The crushing was performed in a custom testing facility between rigid platens which can be moved independently in two orthogonal directions. The facility allows testing at various biaxiality ratios and volume reductions as high as 95%. The facility was used to conduct several series of biaxial crushing experiments on nearly square honeycomb specimens (18×21 cells). In each experiment we recorded the true stress–displacement responses in the x- and y-directions as well as full field views of the deformation using a video camera. Biaxial crushing is quite complex and the prevalent mechanisms of collapse depend on the biaxiality ratio (γ). As is the case in uniaxial crushing, the onset of collapse involves localized instabilities, however, the extent of localized deformation varies with γ. The energy absorption capacity of the material depends on γ. The highest energy is required when the specimen is crushed at the same rates in the two directions.

1. Introduction

Two-dimensional cellular materials such as honeycombs exhibit mechanical characteristics representative of many space filling cellular materials. Because of this they have been used as models to study the mechanical behavior of this class of materials (e.g. Shaw and Sata, 1966; Patel and Finnie, 1970; Gibson et al., 1982; Ashby, 1983; Gibson and Ashby, 1997; Klintworth and Stronge, 1988; Zhang and Ashby, 1992; Warren and Kraynik, 1987; Warren et al., 1989; Papka and Kyriakides, 1994, 1988c; Prakash et al., 1996; Triantafyllidis and Schraad, 1998). In a preceding

* Corresponding author. Fax: 001 512 471 5500; e-mail: skk@mail.utexas.edu

0020-7683/99/$ - see front matter
PII: S0020-7683(98)00224-8

publication (Papka and Kyriakides, 1998a), we presented the results of a study on in-plane uniaxial crushing of a polycarbonate honeycomb with circular cells. It was shown that the initiation of crushing is due to a shear-type instability of the cells. The instability leads to localization of crushing into a narrow zone involving a few rows of cells. Under displacement-controlled loading, the crushing propagates in a row-by-row fashion while the average stress remains relatively constant. The stress plateau is terminated when all the cells have collapsed and the now densified material recovers significant stiffness. It was demonstrated that with proper modeling of the prevalent nonlinearities of geometry, material, and contact, all aspects of this behavior could be simulated numerically.

A natural extension of this work is the investigation of the behavior of the honeycomb under biaxial crushing which is addressed in the present series of two papers (see also Papka and Kyriakides, 1998b; Papka, 1998). The same polycarbonate honeycomb is now crushed simultaneously in two orthogonal directions between rigid plates. In Part I, we first present a novel biaxial testing facility developed for the special needs of this type of experiment. We subsequently discuss in detail the characteristics of force–displacement responses measured in biaxial crushing experiments of various biaxiality ratios. In Part II, we present results from full scale numerical simulations of these experiments and discuss the challenges that must be overcome for the predictions to be in good agreement with the corresponding experimental results.

2. Biaxial crushing testing facility

The cellular materials of interest typically have densities which are only 1–8% that of the base material. For example, our honeycomb has a density of 5.25 lb/ft^3 (84.1 kg/m^3) which is 7.06% of the density of the polycarbonate from which it is made. Thus, unlike more conventional structural materials, cellular materials can be compressed down to small fractions of their original volume. We designed and built a custom biaxial crushing machine (BICRUMA) capable of meeting this special requirement. A photograph of the BICRUMA is shown in Fig. 1a while its main components are identified in the scaled drawing in Fig. 1b.

The test specimen is compressed by the relative motion of four rigid blocks which surround the test section. This is achieved by employing twelve, low profile, stiff linear motion systems (slides) shown in the figures. The blocks are moved by two independent, orthogonal hydraulic actuators run by closed-loop servo-controllers. The moving parts of the facility are mounted on a stiff frame made of structural tubing.

The test specimen is in smooth contact with four lubricated platens (hardened and ground). Each axis has a load capacity of 10 kips (45 kN) and an initial gage length of 5.25 in (133 mm). Each side of the gage length can be reduced to approximately 24% of its original size. Thus, the volume of the test section can be reduced down to nearly 5.5% of its original value.

The motion of the blocks is accomplished via hydraulic actuators operated by closed-loop controllers. The control system and parts of the hydraulic system are shown schematically in Fig. 2. Each axis can be operated under load or displacement control. The experiments described here were conducted under displacement control at selected velocity ratios (biaxiality ratio, γ)

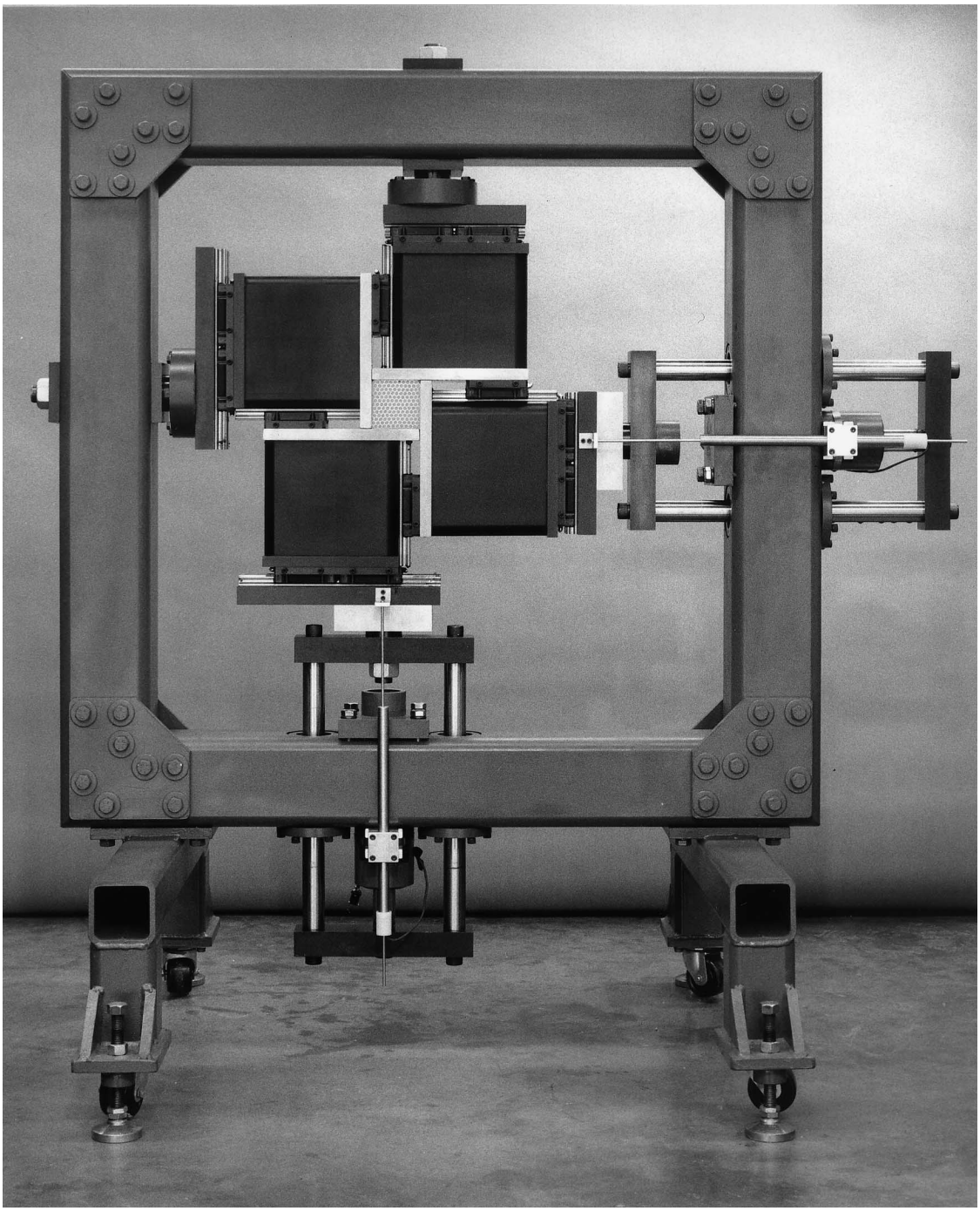

Fig. 1a. Photograph of biaxial crushing machine (BICRUMA).

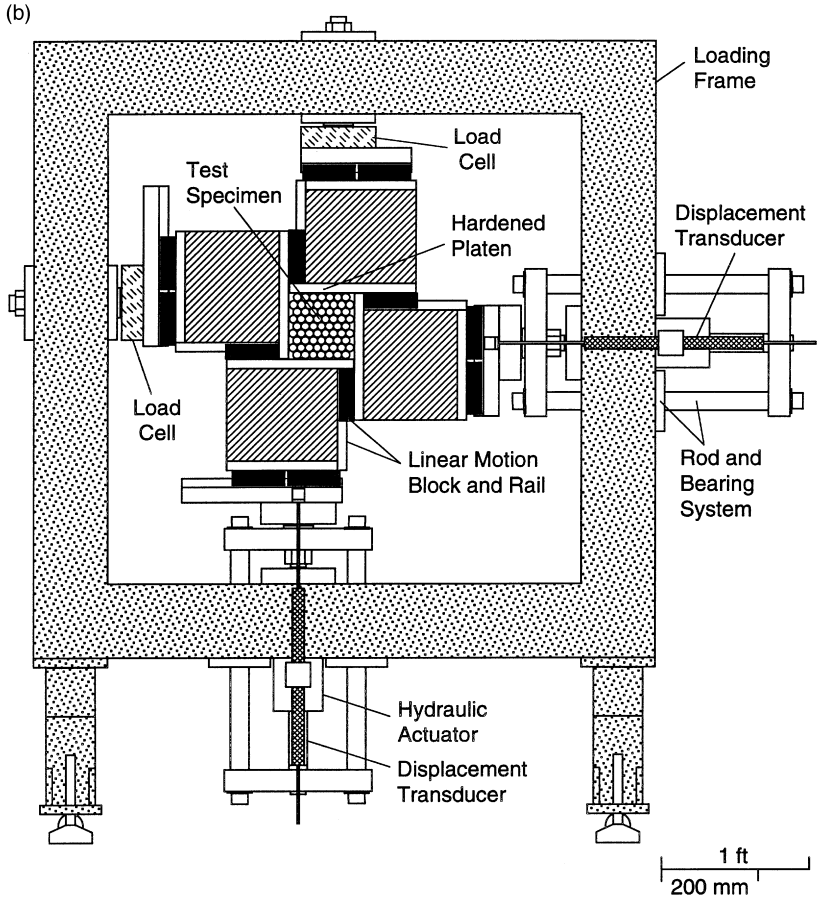

Fig. 1b. Scaled drawing of biaxial crushing machine in which major components are identified.

$$\gamma = \frac{\dot{\delta}_y/b}{\dot{\delta}_x/a} \tag{1}$$

where a and b are the initial dimensions of the test specimen $\{\delta_x, \delta_y\}$ are the applied changes in these dimensions and $(\dot{\delta})$ denotes a velocity (for brevity let $\dot{\bar{\delta}}_x \equiv \dot{\delta}_x/a$ and $\dot{\bar{\delta}}_y \equiv \dot{\delta}_y/b$). Thus, a test is defined by parameters $\{a, b, \gamma, \dot{\bar{\delta}}_x\}$. For example, $\{a = b, \gamma = 1, \dot{\bar{\delta}}_x = 10^{-3}\ \mathrm{s}^{-1}\}$ represents a test on a square specimen compressed at equal rates in the two directions (along diagonal in $\bar{\delta}_x$–$\bar{\delta}_y$ plane in Fig. 3a ≡ equibiaxial test). In the current machine configuration, equibiaxial crushing could be performed at displacement rates up to 3 in/s (75 mm/s). The motion of the blocks during such a test is illustrated by the four machine configurations shown in Fig. 3b. Note that as a result of the novelty of the operation of the machine, the center of the test section moves in the plane of actuation.

The machine can, of course, also be used for uniaxial crushing tests by keeping one of the actuators fixed. In such cases, the test specimen size must be such that lateral contact with the

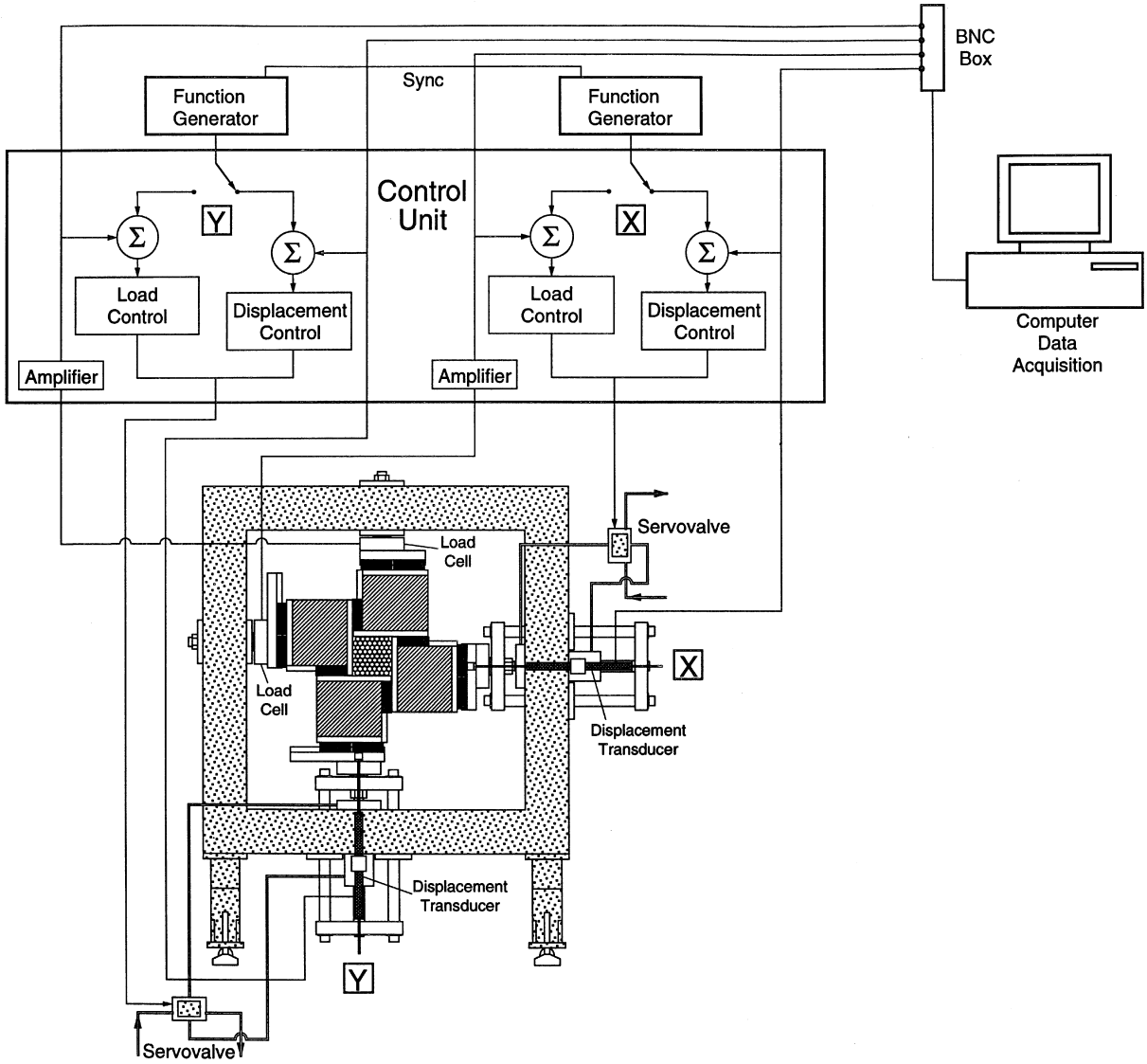

Fig. 2. Schematic of feedback control loops and data acquisition system of BICRUMA.

fixed plates does not take place. By contrast, uniaxial confined tests (i.e., $\gamma = 0$ and $\gamma^{-1} = 0$) are performed by making the specimen the same size as the test section.

Important issues to the proper operation of the machine are machine stiffness and low friction. High stiffness was achieved by the design of the components and by the stiffness characteristics of the slides. The choice of slides and the inclusion of appropriate alignment adjustments in the design resulted in relatively low friction between the moving components. When properly aligned, the machine friction is down to a few pounds ($\sim$5–10 lbf—22–45 N) in each direction. In order to

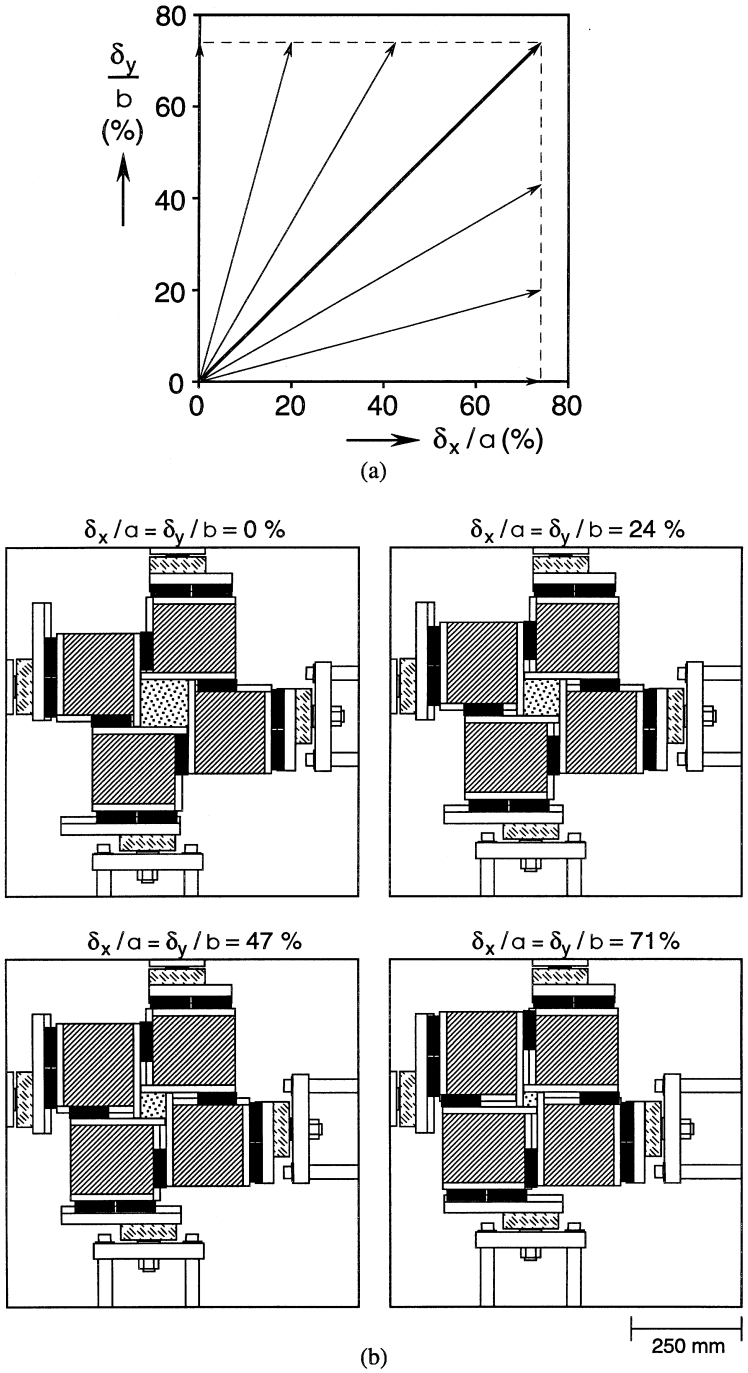

Fig. 3. (a) Radial displacement paths used in experiments. (b) Sequence of configurations demonstrating the motion of the blocks in the BICRUMA during an equibiaxial test.

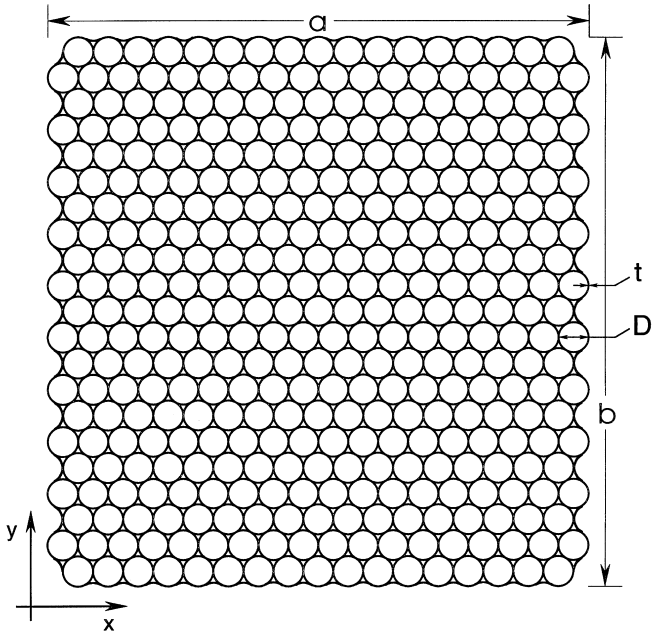

Fig. 4. Geometry of honeycomb specimens used in biaxial experiments.

negate the effect of these small misalignments and frictional forces, the machine was first taken through the displacement history of each test with the test section empty. The forces registered by the load cells were recorded and then subtracted from the corresponding load histories of the actual test. Careful evaluation of this process verified its validity.

The global deformation variables are the platen displacements which are monitored by displacement transducers. A computer operated data acquisition system is used to record the loads (two signals) and displacements (two signals). A video camera and a video recorder are used to provide full field monitoring of the deformation of the specimen. The video and data acquisition systems are synchronized so that the two sets of results can be related.

3. Experimental results

The honeycomb used in the experiments has circular cells in a hexagonal arrangement. It is made from extruded polycarbonate tubes with a diameter (D) of 0.274 in (6.96 mm) and an average wall thickness (t) of 5.68×10^{-3} in (144 μm). The tubes are bonded to each other along arcs spanning 10.5° (mean value). Uniaxial and biaxial experiments have been conducted on 1.25 in (32 mm) thick honeycomb specimens cut from larger sheets of the material. For the purposes of this study we define an orthogonal set of axes (x, y) as shown in Fig. 4. Before discussing results from biaxial experiments, we start with a review of the uniaxial crushing responses in the x- and y-direction.

3.1. Uniaxial crushing

Uniaxial crushing of finite size honeycomb specimens in the y-direction was extensively discussed in Papka and Kyriakides (1998a). Here we review results from a test on a specimen with 10 columns and 15 rows of cells crushed at a normalized displacement rate of $5 \times 10^{-3}\ s^{-1}$. Figure 5a shows a plot of the average stress ($\sigma_y \equiv$ load/initial cross sectional area) against the normalized applied displacement ($\bar{\delta}_y$). The sequence of deformed configurations in Fig. 5b correspond to the equilibrium states identified on the response. This uniaxial response has the general features common to many cellular materials (e.g., see Gibson and Ashby, 1997). Initially, it is relatively stiff and nearly linear. Each cell deforms symmetrically about a vertical axis passing through its center and deformation is essentially uniform throughout the specimen (configuration ①). At a stress of approximately 7 psi (48 kPa), the response begins to soften and eventually a limit load develops at a stress of $\gamma_{Iy} = 8.6$ psi (59 kPa) and a strain of $\varepsilon_{Iy} = 7.2\%$ ($I \equiv$ initiation). Beyond the limit load, deformation localizes into a narrow, horizontal zone involving cell rows 11 and 12 (see ②). The cells in these rows collapse in an unsymmetric, shear-type mode while cells outside this zone remain symmetrically deformed. As the collapse of the two rows progresses, deformation spreads to the neighboring rows. Eventually, contact between the walls of the collapsed cells arrests deformation in rows 11 and 12.

This spreading of collapse from row-to-row continues creating an undulating stress plateau (configurations ④–⑦). By configuration ⑦, all cells have collapsed except for those next to the loading plates. At this point the stress starts to increase again (behavior reminiscent of propagating instabilities which can affect some large scale structures discussed in Kyriakides, 1994). The propagation of collapse involves the same shear-type mode which causes the initial instability. Figure 6 shows close-up views of a characteristic cell in the process of collapsing. The undeformed configuration is identified as [0]. Initially, the cell deforms symmetrically (see [1]) but then switches

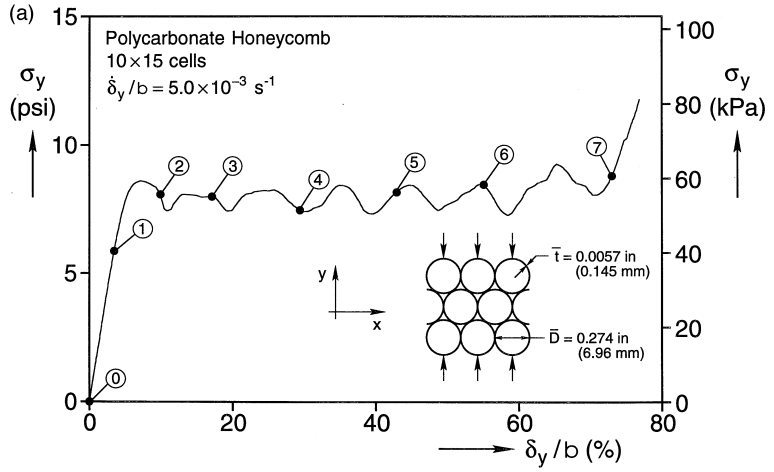

Fig. 5a. Stress–displacement crushing response of honeycomb in a uniaxial crushing test in the y-direction.

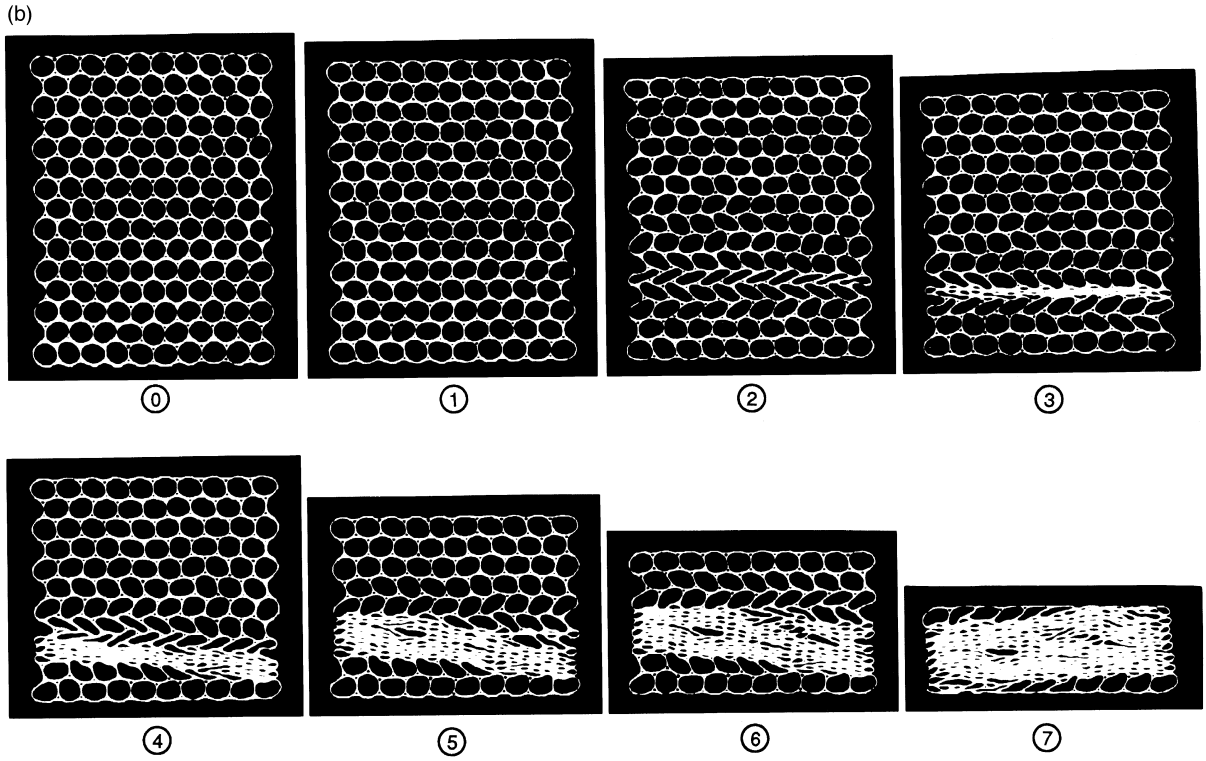

Fig. 5b. Sequence of deformed configurations corresponding to response in Fig. 5a.

to the unsymmetric mode seen in 2. Configurations 3 and 4 show the cell at increasing stages of collapse while in 5 the cell walls come into contact arresting further local deformation.

Although not obvious from Fig. 5b, the video recording clearly showed that the propagating front of collapse usually involved two adjoining rows of cells. Furthermore, each stress undulation corresponds to the collapse of a pair of rows. Therefore, specimens of this height typically exhibited seven stress hills and seven stress valleys across the plateau. In this particular case, the plateau terminates at $\bar{\delta}_y = 70\%$. The average stress of the plateau, which will be called propagation stress (σ_{Py}), is 8.0 psi (55.2 kPa). We define the difference between the initiation strain and the value at the termination of the plateau as the extent of the plateau ($\Delta\varepsilon_{Py}$) which for this case has a value of 62%. The energy absorption capacity of the material per unit undeformed volume, $\mathscr{E}_y$, is the integral under the response up to the densification point ($\bar{\delta}_y \in [0, 0.70]$). In this case $\mathscr{E}_y = 5.33$ psi (36.6 kPa).

The location of initiation of collapse in the specimen is influenced by small geometric imperfections. As a result, the order of events during crushing varied somewhat from experiment to experiment. However, the repeatability of the propagation stress and the extent of the plateau was excellent (Papka and Kyriakides, 1998a).

As pointed out in Papka and Kyriakides (Section 4.4, 1998a), the elastic properties of such honeycombs are strongly influenced by edge effects and specimen size. In order to limit the influence

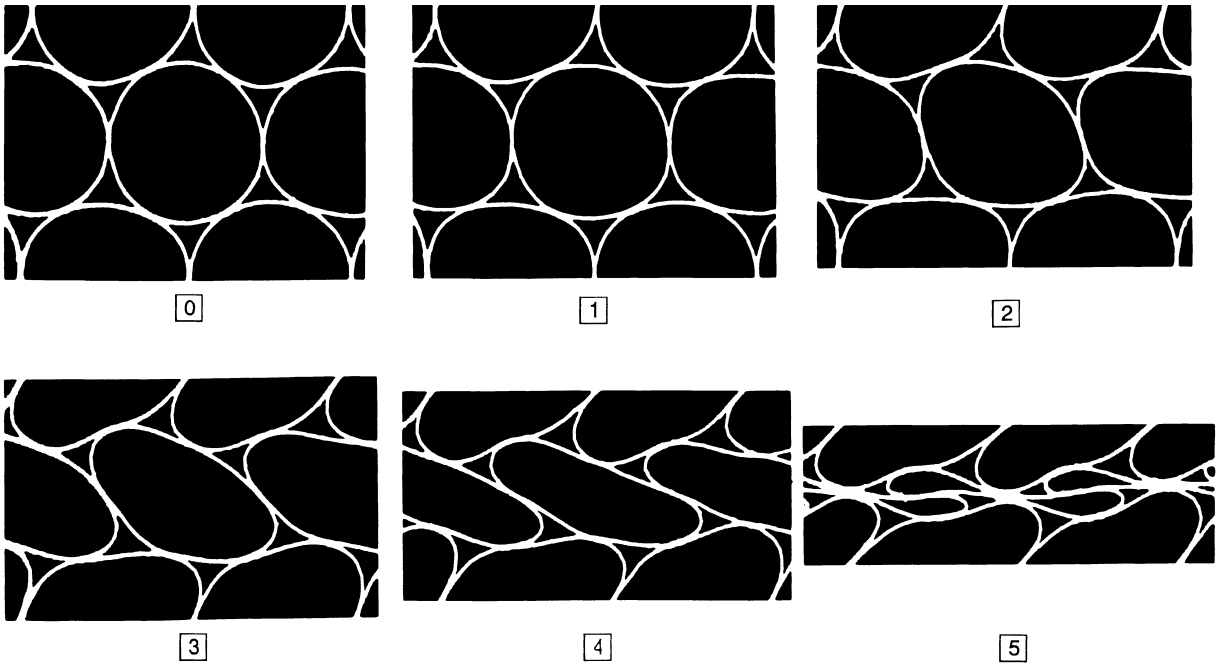

Fig. 6. Close-up views of collapse configurations of a honeycomb cell in a y-crushing test.

of these effects, the elastic moduli in the x- and y-directions were measured in separate experiments involving nearly square specimens with 49×59 cells. The stress was assumed to be uniformly distributed while the strain was measured in the middle of the specimens using a two-inch (51 mm) gage length extensometer. The elastic modulus, E_y^*, was found to be 240 psi (1.66 MPa).

The uniaxial crushing response in the x-direction on a specimen with 11×13 cells is shown in Fig. 7a. The corresponding response in the y-direction is included for comparison purposes. A set of corresponding deformed configurations are shown in Fig. 7b. The σ_x–$\bar{\delta}_x$ response is similar to the one in the y-direction except that the stress plateau is somewhat higher and exhibits more nonlinearity prior to the load maximum. This is partly due to the early collapse of some of the cells directly in contact with the platens well before instability initiates in the rest of the specimen (see ①). The collapse of these edge cells also influences the initiation of instability. It takes place at a stress of 10.5 psi (72.3 kPa) and is less distinct than it was for the tests in the y-direction. The influence of these edge effects is highlighted by the fact that some of the subsequent events require a somewhat higher stress than the initiation stress.

The nature of the instability seen in configuration ② is also different. Once again, deformation localizes in distinct bands of cells but, in this case, the bands are inclined at angles of approximately $\pm 60\%$ to the x-axis (in the undeformed configuration). These happen to be two of the three directions in which cells are aligned. More details of the collapse mechanism can be seen in the close-up views of a cluster of cells shown in Fig. 8. The mechanism involves simultaneous ovalization (1 and 2) and shearing (4 and 5) of inclined rows of cells. Because of the cell alignment, inclined

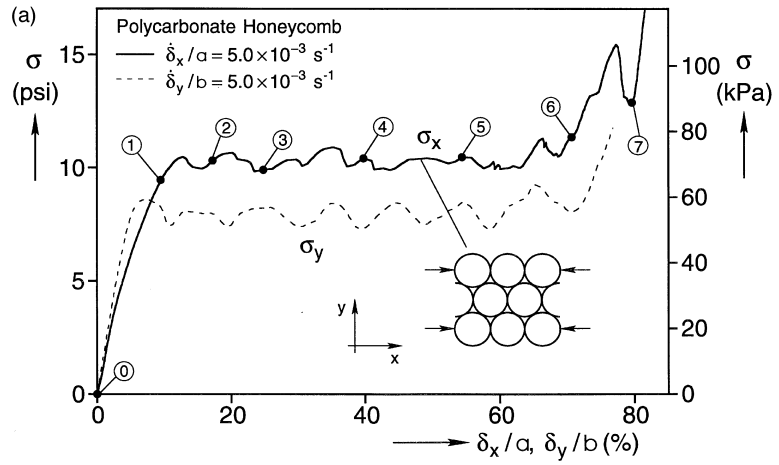

Fig. 7a. Stress–displacement crushing response of honeycomb in a uniaxial crushing test in the x-direction.

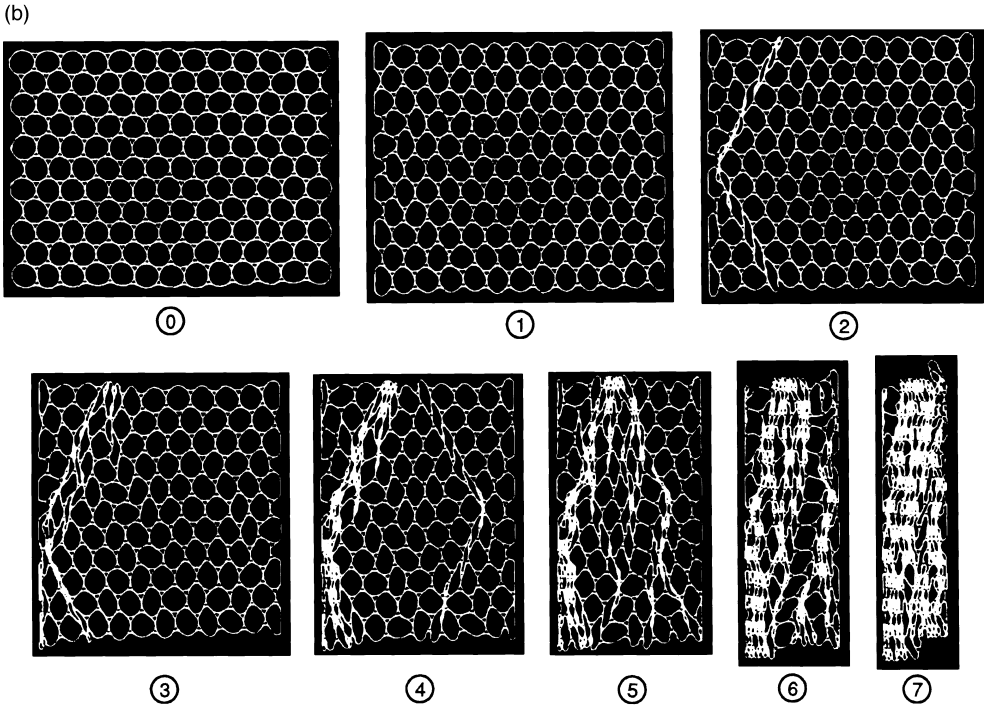

Fig. 7b. Sequence of deformed configurations corresponding to response in Fig. 7a.

rows of cells collapse almost entirely without affecting their neighbors significantly. Thus, it seems that in this mechanism, initiation of instability at a different site in the specimen is easier. As a

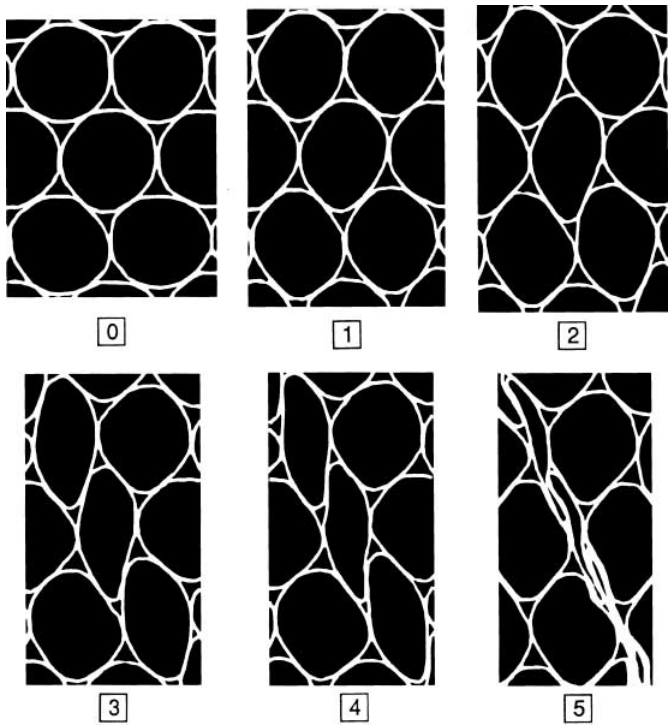

Fig. 8. Close-up views of collapse configurations of a honeycomb cell in an x-crushing test.

result, the events are more randomly distributed in the specimen and the regular stress undulations seen in Fig. 5a are absent. For example, in configuration ④ instability initiated at two new sites on the RHS of the specimen in the same two directions but the zones are now mirror images of the two initial ones. This sequence of events continues and, in the process, a relatively flat stress plateau is traced. The progression of events was such that one zone of cells seen in configuration ⑥ has remained relatively undeformed. As a result of deformation incompatibilities with the collapsed cells surrounding it, collapse of this zone requires a higher level of stress represented by the last stress peak in the response. By configuration ⑦, the whole specimen has collapsed and the response takes a steep upturn.

The elastic modulus in the x-direction was again measured in separate experiments on 49×59 cell specimens in the fashion described above. Here, in addition to sensitivity to size, we found the measurement of elastic modulus to be very sensitive to how parallel the edges in contact with the platens were. In this direction, the cells align with the applied force (see Fig. 4). As a result, load nonuniformities at the edges do not diffuse into the specimen as easily as in the y-direction where cells are staggered in the direction of the applied load. The modulus, E_x^*, measured was 236 psi (1.63 MPa) confirming the initial elastic isotropy imposed to the material by the hexagonal symmetry of the microstructure.

The major material parameters are listed in Table 1. The propagation stress, σ_{Px}, is 27% larger than σ_{Py}. The extent of the stress plateau is approximately the same and the strain energy absorption

Table 1
Comparison of problem variables measured in uniaxial crushing tests in the x- and y-directions

x-direction					y-direction				
$E_x^{*\dagger}$ psi (MPa)	σ_{Ix} psi (kPa)	σ_{Px} psi (kPa)	$\Delta\varepsilon_{Px}$ (%)	$\mathscr{E}_x$ psi (kPa)	E_y^* psi (MPa)	σ_{Iy} psi (kPa)	σ_{Py} psi (kPa)	$\Delta\varepsilon_{Py}$ (%)	$\mathscr{E}_y$ psi (kPa)
236 (1.63)	10.5 (72.3)	10.2 (70.5)	63.6	6.69 (46.1)	240 (1.66)	8.6 (59.3)	8.0 (55.2)	63.1	5.31 (36.6)

† Measured in a 49×59 cell specimen.

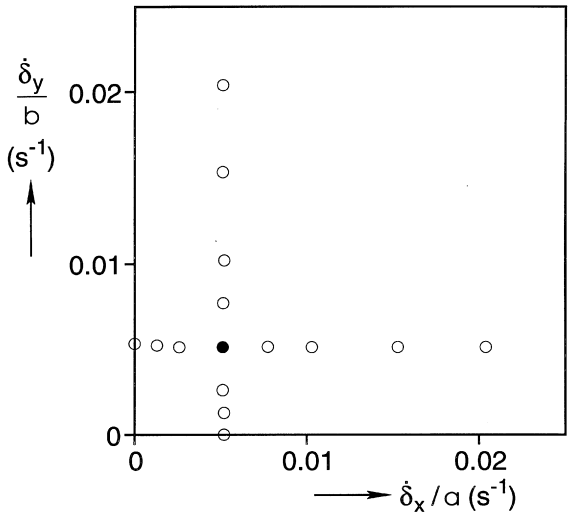

Fig. 9. Displacement rate in the y-direction vs displacement rate in the x-direction used in the two series of biaxial tests conducted.

capacity, $\mathscr{E}_x$, is approximately 26% higher than the value measured in the y-direction ($\mathscr{E}_x \equiv$ integral under response for $\bar{\delta}_x \in [0, 0.70]$).

3.2. Biaxial crushing experiments

We now present results from a set of biaxial experiments conducted in the BICRUMA. The test specimens dimensions were approximately $a \times b = 5.04 \times 5.16$ in (128×131 mm–18×21 cells). The edges and the corners were trimmed as shown in Fig. 4 to reduce friction and edge effects. In addition, a lightweight grease was applied to the platens and the edges of the specimens.

We start with two series of tests conducted at the biaxial displacement rates shown in Fig. 9. In the first series, the displacement rate in the x-direction was fixed at $\dot{\bar{\delta}}_x = 5 \times 10^{-3}\ \mathrm{s}^{-1}$ while the rate in the y-direction was assigned eight different values in the range of $\dot{\bar{\delta}}_y \in [0, 2 \times 10^{-2}]\ \mathrm{s}^{-1}$; in other

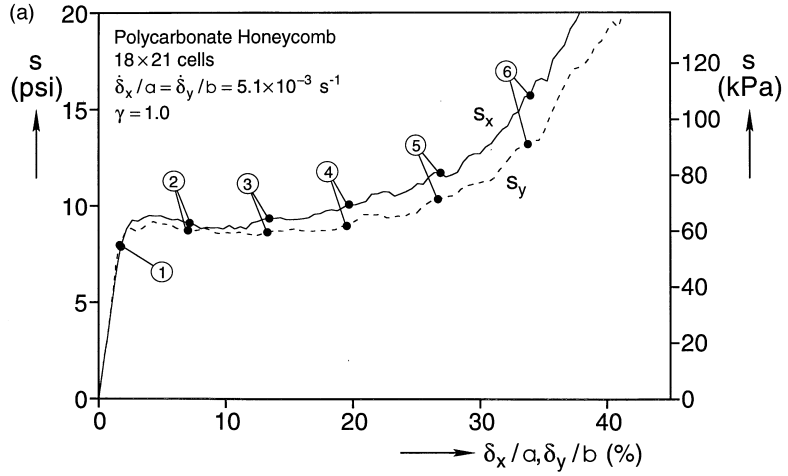

Fig. 10a. True stress–displacement responses of equibiaxial experiment.

words, the biaxiality ratio was varied in the range of $\gamma \in [0,4]$. In the second series of eight experiments, the displacement rate in the y-direction was fixed at $\dot{\bar{\delta}}_y = 5\times10^{-3}$ s^{-1} while the rate in the x-direction was varied in the range of $\dot{\bar{\delta}}_x \in [0, 2\times10^{-2}]$ s^{-1}. Thus, in this case the biaxiality ratio varied in the range of $\gamma^{-1} \in [0,4]$. The events and results are strongly dependent on the biaxiality ratio and to a lesser degree on the rate of loading. The richness in the underlying collapse mechanisms will be illustrated through several examples from the two sets of experiments.

The results reported will be influenced to some degree by two unavoidable factors, friction and edge effects. Despite the lubrication applied, friction between the edges of the specimens and the steel platens could not be completely avoided. Coulomb friction coefficients in the range 0.1–0.15 were measured in experiments conducted for this purpose (Papka, 1998). The effects of the edges and corners on the recorded behavior will become apparent from the results that follow.

3.3. *Equibiaxial test*: $\gamma = 1.0$, $\dot{\bar{\delta}}_x = 5.1\times10^{-3}\, s^{-1}$

We first consider a case where the specimen was crushed simultaneously in the x- and y-directions at the same rate. In such biaxial experiments, the cross sectional area of the specimen can undergo large changes. Therefore, true stresses will be reported and will be designated by s_x and s_y. Figure 10a shows plots of s_x and s_y vs the respective applied normalized displacements $\bar{\delta}_x$ and $\bar{\delta}_y$. Figure 10b shows a sequence of deformed configurations corresponding to the points identified on the responses.

Initially, the material is elastic and exhibits a stiff and stable response where the cells deform essentially uniformly and the deformation of each cell is symmetric about the x- and y-axes. Exceptions to this are the two vertical edges of the specimen which are seen to be crushed more significantly and, to a lesser extent, the top and bottom edges which exhibit a small gradient in deformation from left to right probably caused by friction. These effects influence the net initial stiffnesses recorded. In the uniaxial tests, the elastic modulus was determined from local strain measurements made in larger specimens. This was difficult to do in the BICRUMA. Thus, the

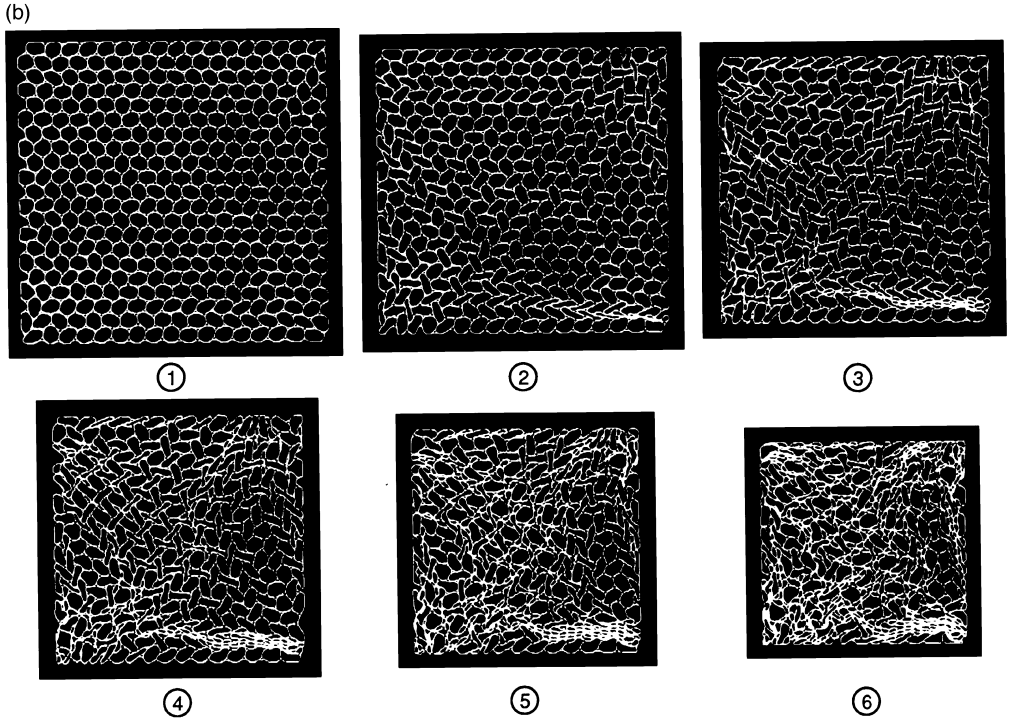

Fig. 10b. Sequence of deformed configurations corresponding to the equibiaxial test Fig. 10a.

initial slopes of the responses presented are based on the global displacement measurements. In this equibiaxial text, the initial elastic stiffnesses in the x- and y-directions are just over two times the values of E_x^* and E_y^* listed in Table 1. This, of course, is expected as the side constraints and the biaxial stresses stiffen the honeycomb.

The elastic regime is terminated by the onset of instability involving a mode of cell deformation which can be clearly seen in configuration ② in Fig. 10b. The initiation stresses converted to engineering stress values for comparison purposes are listed in Table 2. They have the same order of magnitude as those measured in the uniaxial tests (Table 1). Continued loading results in the formation of fascinating regular patterns seen in configurations ③–⑥. The deformation is not uniform throughout the specimen for reasons that are discussed below. However, a significant part of it behaves much like the cluster of cells shown in the close-up views in Fig. 11. For a significant part of the deformation history, the central cell (pivot) of a seven cell hexagonal cluster remains relatively undeformed. The surrounding cells develop a shear-type deformation resulting in the twisting pattern seen at various degrees of deformation in configurations [1]–[5]. Through this pattern, the deforming honeycomb maintains approximately hexagonal symmetry but at a different level. Now the corners of the hexagon (the pivots) are alternate cells in the three original directions of symmetry. The intermediate cells are those which undergo the twisting deformation. In this case, several of the pivot cells remain essentially circular up to global strains of about 35% (e.g. in configuration [5] in Fig. 11, $\bar{\delta}_x$ and $\bar{\delta}_y$ are approximately 35%).

This regular pattern is broken up in several places by localized collapse such as that seen in the

Table 2a
Problem variables measured in biaxial experiments of various values of γ and $\dot{\delta}_x = 5 \times 10^{-3}\ s^{-1}$

$\dot{\delta}_x\ s^{-1}$	$\dot{\delta}_y\ s^{-1}$	γ	σ_{Ix} psi (kPa)	σ_{Iy} psi (kPa)	$\mathscr{E}_x$ psi (kPa)	$\mathscr{E}_y$ psi (kPa)	$\mathscr{E}$ psi (kPa)
5.1×10^{-3}	0	0	10.2	6.87	6.29	0	6.29
			(70.3)	(47.4)	(43.4)		(43.4)
5.2×10^{-3}	1.3×10^{-3}	0.25	10.3	7.08	5.77	0.81	6.58
			(71.0)	(48.8)	(39.8)	(5.59)	(45.4)
5.1×10^{-3}	2.6×10^{-3}	0.51	9.59	8.49	4.97	1.84	6.81
			(66.1)	(58.6)	(34.2)	(12.7)	(47.0)
5.1×10^{-3}	5.1×10^{-3}	1.0	9.19	8.80	3.64	3.23	6.87
			(63.4)	(60.7)	(25.1)	(22.3)	(47.4)
5.1×10^{-3}	7.7×10^{-3}	1.51	8.41	9.11	2.54	3.86	6.40
			(58.0)	(62.8)	(17.5)	(26.6)	(44.1)
5.2×10^{-3}	10.2×10^{-3}	1.96	7.56	9.17	1.81	4.20	6.01
			(52.1)	(63.2)	(12.5)	(29.0)	(41.4)
5.1×10^{-3}	15.4×10^{-3}	3.01	7.17	9.53	1.19	4.60	5.79
			(49.4)	(65.7)	(8.21)	(31.7)	(39.9)
5.1×10^{-3}	20.4×10^{-3}	4.0	6.52	9.80	0.884	4.92	5.80
			(45.0)	(67.6)	(6.10)	(33.9)	(40.0)

Table 2b
Problem variables measured in biaxial experiments of various values of $1/\gamma$ and $\dot{\delta}_y = 5 \times 10^{-3}\ s^{-1}$

$\dot{\delta}_x\ s^{-1}$	$\dot{\delta}_y\ s^{-1}$	$1/\gamma$	σ_{Ix} psi (kPa)	σ_{Iy} psi (kPa)	$\mathscr{E}_x$ psi (kPa)	$\mathscr{E}_y$ psi (kPa)	$\mathscr{E}$ psi (kPa)
0	5.0×10^{-3}	0	4.82	9.88	0	5.35	5.35
			(33.2)	(68.1)		(36.9)	(36.9)
1.3×10^{-3}	5.2×10^{-3}	0.25	6.36	10.1	0.848	4.94	5.79
			(43.9)	(69.7)	(5.85)	(34.1)	(39.9)
2.6×10^{-3}	5.1×10^{-3}	0.51	7.65	9.03	1.85	4.31	6.16
			(52.8)	(62.3)	(12.8)	(29.7)	(42.5)
5.1×10^{-3}	5.1×10^{-3}	1.0	9.19	8.80	3.64	3.23	6.87
			(63.4)	(60.7)	(25.1)	(22.3)	(47.4)
7.9×10^{-3}	5.2×10^{-3}	1.51	9.67	8.65	4.32	2.49	6.81
			(66.7)	(59.7)	(29.8)	(17.2)	(47.0)
10.3×10^{-3}	5.1×10^{-3}	2.02	10.1	8.63	4.70	1.84	6.54
			(69.7)	(59.5)	(32.4)	(12.7)	(45.1)
15.3×10^{-3}	5.1×10^{-3}	3.0	9.70	7.80	5.62	1.07	6.69
			(66.9)	(53.8)	(38.8)	(7.38)	(46.1)
20.4×10^{-3}	5.1×10^{-3}	4.0	9.70	7.64	5.79	0.835	6.63
			(66.9)	(52.7)	(39.9)	(5.76)	(45.7)

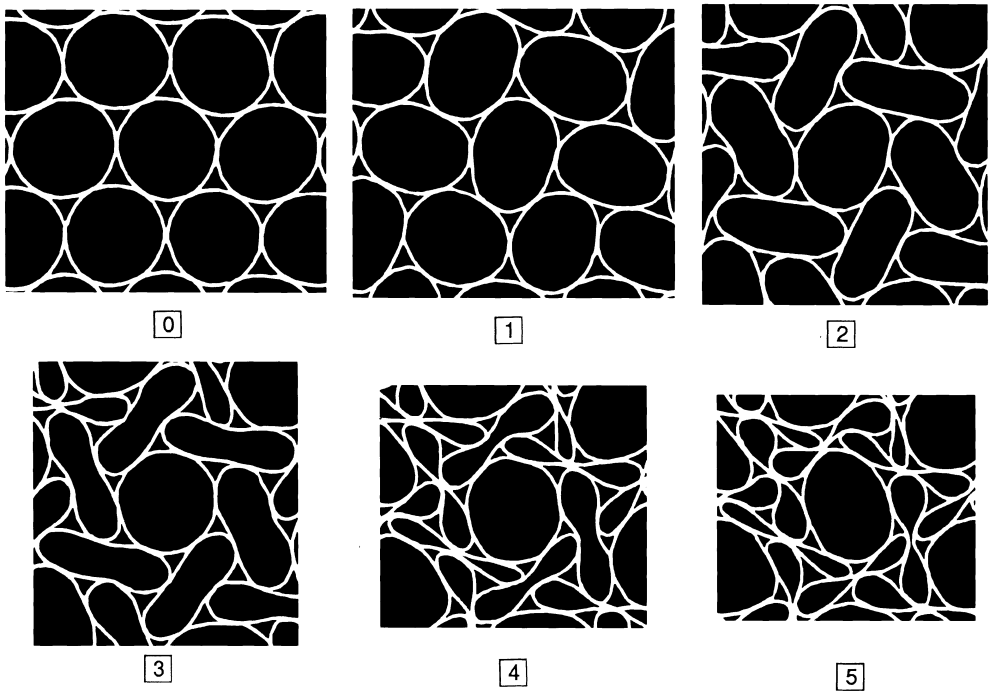

Fig. 11. Deformation patterns of a cluster of cells during an equibiaxial experiment.

lower part of configuration ② in Fig. 10b and at the edges of the specimen. There are three contributors to this localized collapse: edge effects, friction, and incompatibility of the preferred mode of deformation with a specimen of finite dimensions. As was the case in the uniaxial test in the x-direction, crushing of the cells along the two vertical edges initiates early in the deformation history. In the neighborhood of the knee in the responses, several 'fingers' of collapse start from these collapsed cells and penetrate the interior of the specimen as seen in the neighborhood of the two upper corners and in the lower right corner in ②. Coupled with these effects are 'stick-slip' conditions which result from friction. In this regard, it is important to point out that the top platen does not move during such a test, the right platen moves only in the x-direction, the left platen moves only in the y-direction, and the bottom platen moves in both directions. Thus, the platens slide along the left and bottom side of the specimen while the specimen slides along the right platen which only moves normal to its loading surface and along the top platen which remains essentially fixed.

During the initial stages of localized crushing, the force–displacement response monotonically decreases. Subsequently, between normalized displacements of 15–25%, they remain relatively flat and beyond 25% they monotonically increase. When the results are converted into true stress–displacement responses, as in Fig. 10a, the extent of nonmonotonicity is masked to some degree. By the time the specimen has been crushed down to approximately 36% of its original volume ($\bar{\delta}_x = \bar{\delta}_y = 0.40$), the material has densified and both responses stiffen quite significantly.

The energy absorption capacity under the present loading conditions was evaluated up to a

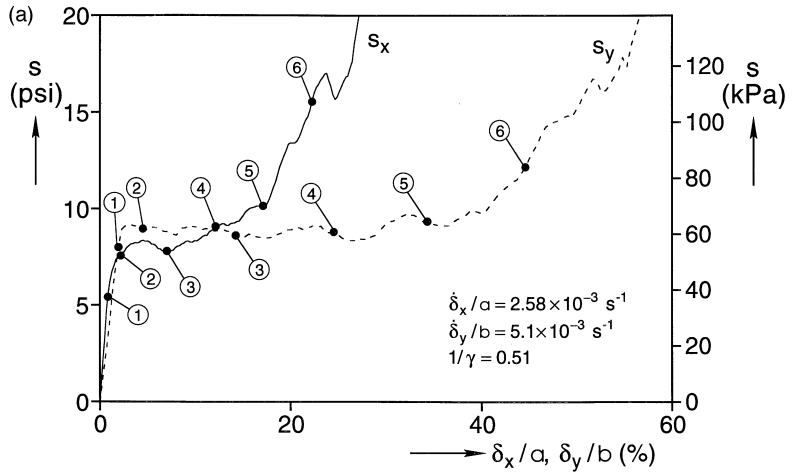

Fig. 12a. True stress–displacement responses from a biaxial crushing test with $\gamma^{-1} = 0.51$.

volume change of 65%. The values for each loading direction ($\mathscr{E}_x, \mathscr{E}_y$) as well as their sum ($\mathscr{E}$) are listed in Tables 2. The energies absorbed up to this deformation level are, respectively, 34 and 45% higher than those measured in the uniaxial crushing tests in the x- and y-directions.

3.4. *Biaxial test*: $\gamma^{-1} = 0.51$, $\dot{\bar{\delta}}_y = 5.1 \times 10^{-3}\, s^{-1}$

We now consider results from a biaxial experiment in which the crushing rate in the y-direction was approximately twice that of the x-direction. The true stress–displacement responses measured are shown in Fig. 12a and a set of corresponding deformed configurations in Fig. 12b. In the early stages of deformation, the behavior is reminiscent of that observed in the uniaxial crushing experiment in the y-direction (Fig. 5). The initiation of instability is via shearing of horizontal rows of cells (see ②) similar to that seen in the uniaxial test. This is partly due to the slower rate at which δ_x is applied but, also, because initially a significant portion of the displacement applied in the x-direction is absorbed by local crushing of the cells at the vertical edges leaving the interior of the specimen relatively undeformed. In fact, $\bar{\delta}_x$ reaches a value of approximately 5% before the effects of the biaxial nature of the crushing start to become apparent. At higher values of $\bar{\delta}_x$, we start to see deformation patterns similar to those of the equibiaxial test (Fig. 11) which remain evident even in configuration ⑥ ($\bar{\delta}_y \approx 45\%$). A sample of this second mode of crushing is shown in the close-up views in Fig. 13. Initially (configurations [1] and [2]), it is very similar to the mode in Fig. 11. At higher strains, the unequal crushing applied in the two directions tends to cause flattening of the pattern in the y-direction. The result of this dichotomy between 'early' and 'later' crushing behavior is the mixture of crushing patterns seen in configurations ④–⑥ in Fig. 12b.

After initiation of instability, the value of s_y remains relatively constant around 9 psi (6.3 kPa) until $\bar{\delta}_y$ reaches 40%. By this time the specimen is significantly crushed and s_y starts to increase.

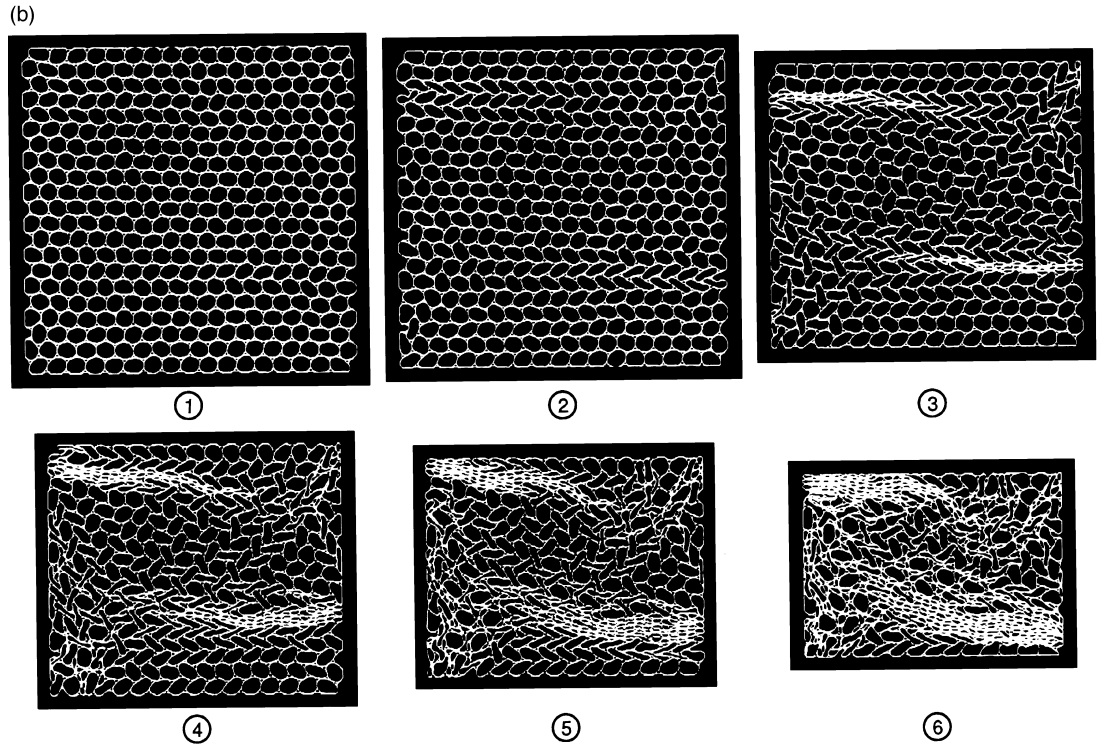

Fig. 12b. Sequence of deformed configurations corresponding to response in Fig. 12a.

The energy absorbed when the specimen is crushed down to 65% of its original volume is 6.16 psi (42.5 kPa) per unit initial volume which is approximately 10% lower than the corresponding value for the equibiaxial test (Table 2b).

3.5. *Biaxial test*: $\gamma^{-1} = 3$, $\dot{\bar{\delta}}_y = 5 \times 10^{-3}\ s^{-1}$

The third biaxial crushing experiment we will examine in detail involves a specimen crushed at $\dot{\bar{\delta}}_y = 5 \times 10^{-3}\ s^{-1}$ while the rate in the x-direction was three times higher. The true stress–displacement responses recorded are shown in Fig. 14a and a set of corresponding deformed configurations in Fig. 14b. In the early stages of deformation (① and ②), we observe deformation patterns aligned with two of the axes of symmetry of the material inclined at $\pm 60^\circ$ to the x-axis. In the x-direction, a load maximum occurs at 9.7 psi (67 kPa) while in the y-direction at 7.8 psi (54 kPa) (note that the two load maxima are coincident in time but differ in displacement by a factor of 3). The x-direction force–displacement response remains monotonically decreasing up to $\bar{\delta}_x \approx 27\%$ and subsequently becomes monotonically increasing. Once again, several fingers of localized deformation which are associated with the $\pm 60^\circ$ directions are observed. At the same time, in the rest of the specimen, an evolution of events takes place which transforms the original primarily inclined deformation patterns into ones with more of a rectangular symmetry. These are clearly seen in the left half of the specimen in configurations ③–⑤.

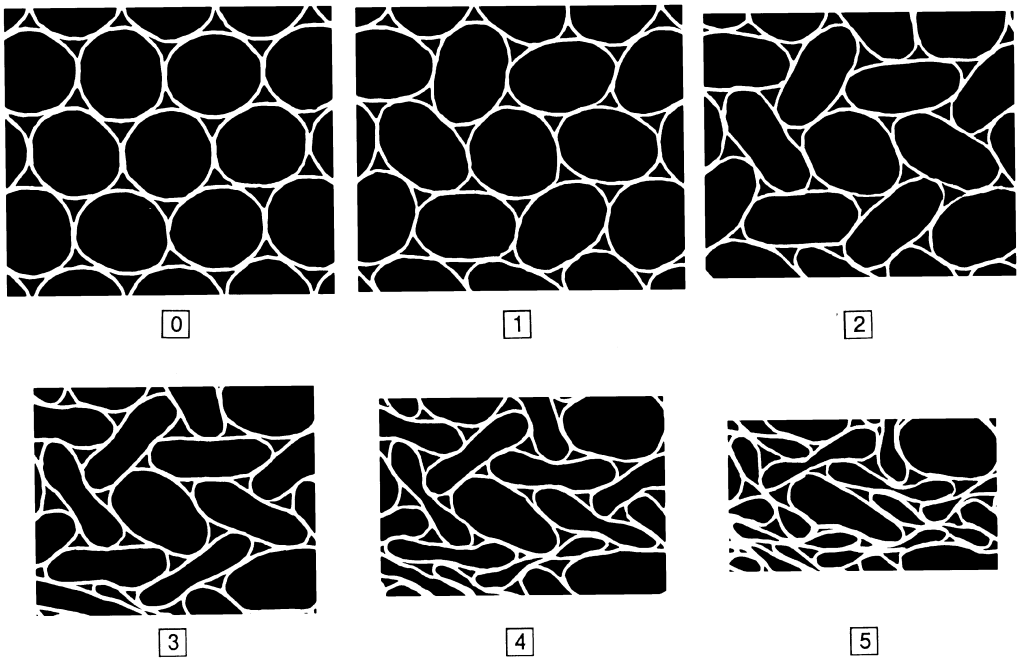

Fig. 13. Deformation patterns of a cluster of cells developed in the experiment in Fig. 12.

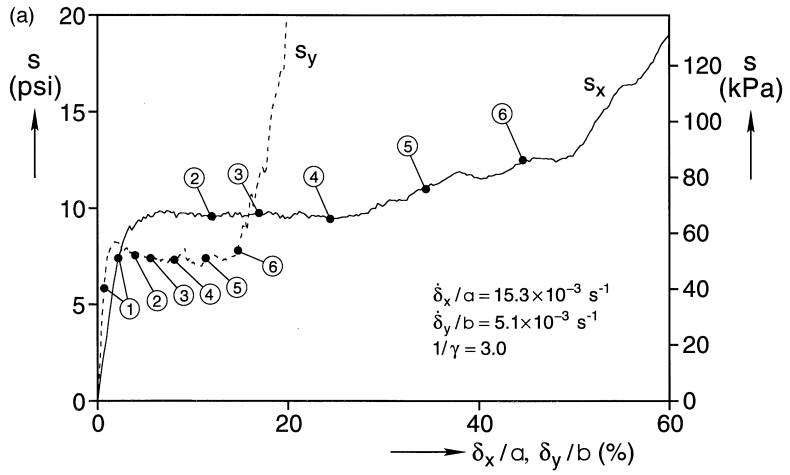

Fig. 14a. True stress–displacement responses from a biaxial crushing test with $\gamma^{-1} = 3$.

The sequence of events that lead to this pattern are seen in more detail in a set of close-up views in Fig. 15. Interestingly, at this site, in the early stages of deformation (configuration 1) the cells

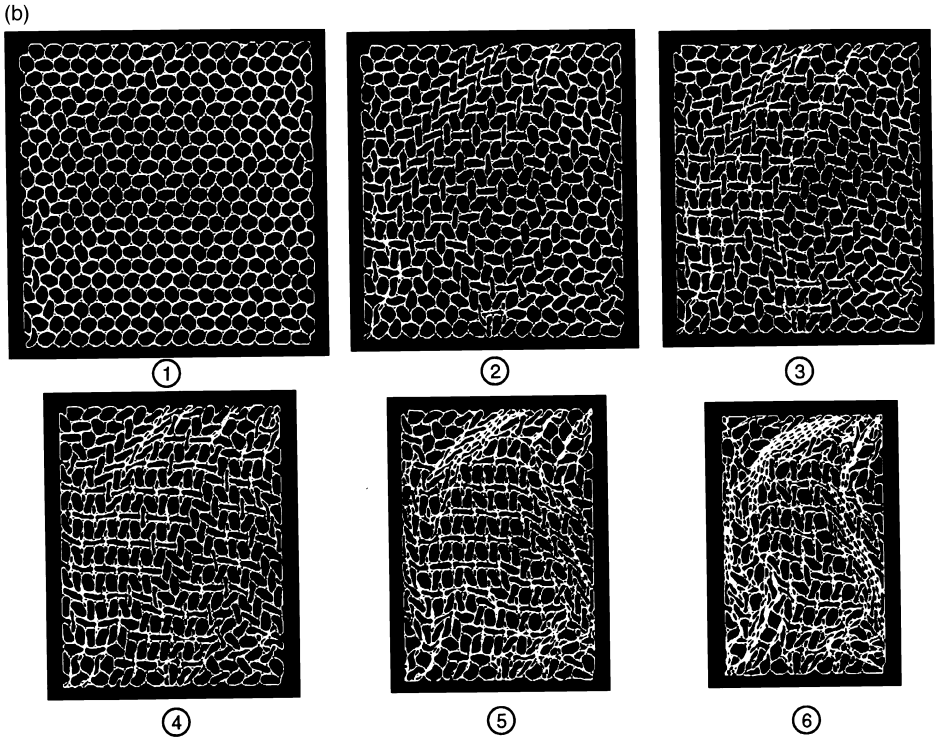

Fig. 14b. Sequence of deformed configurations corresponding to response in Fig. 14a.

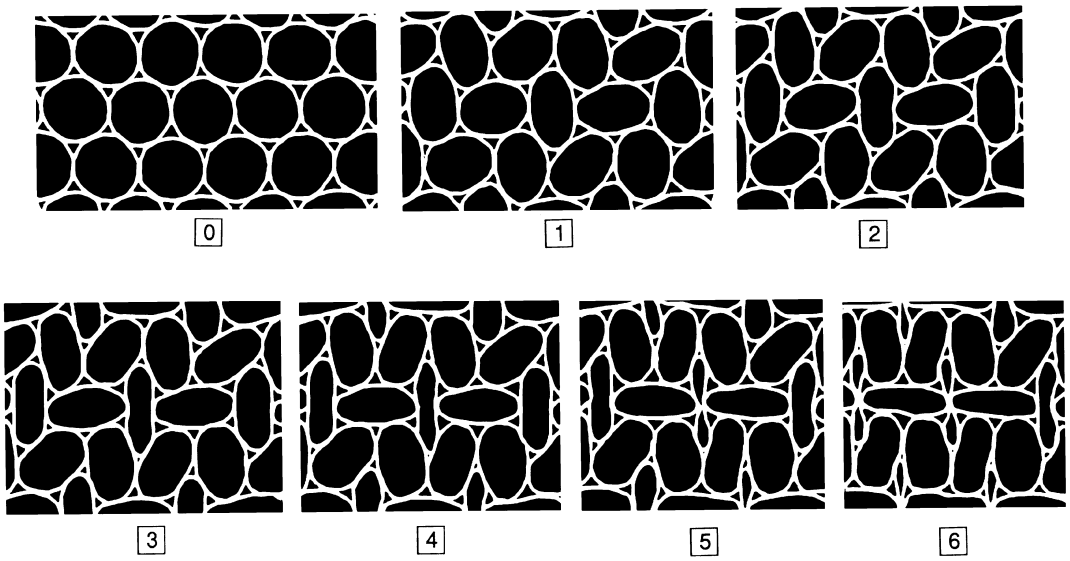

Fig. 15. Deformation patterns of a cluster of cells developed in the experiment in Fig. 14.

exhibit the hexagonal twisting pattern seen in the experiment with $\gamma = 1$. In configuration 2, the alignment of deformation in the $\pm 60^\circ$ directions starts to become apparent while configurations 3 and 4 illustrate its transformation to the more rectangular pattern. The latter is seen fully developed in configurations 5 and 6. Alternate horizontal rows of cells have accommodated the x-displacement by flattening in that direction. The y-displacement is accommodated in the intermediate rows of cells. In these rows, alternating cells have collapsed in the x- and y-directions. The ones that collapse in the x-direction squeeze themselves into the two neighboring rows. The pattern when fully developed has approximately a deformation ratio which is closer to 4:1, which is somewhat higher than the imposed value. This, of course, results from the fact that the deformation is not uniform throughout the specimen. Indeed, this characteristic is common to most of the biaxial tests performed. As a result, the patterns assigned above to particular values of γ and γ^{-1} were seen to also occur locally in experiments of different biaxiality ratios.

By the time the specimen has been crushed down to $\bar{\delta}_x \approx 40\%$, the material is quite densified, the response is on the rise and the patterns break up. The energy absorbed when the specimen is crushed down to 65% of its original volume is 6.69 psi (46.1 kPa—Table 2b).

3.6. Broader variation of biaxiality ratios

The effect of the biaxiality ratio on the mechanical behavior of the honeycomb was further explored in additional experiments making up two sets in which the displacement combinations shown in Fig. 9 were used. Each set includes eight independent experiments and both have the equibiaxial test in common. Results from the remaining twelve experiments will be presented in a summarized fashion,

Figure 16 shows the true stress–displacement responses from six of the eight experiments in which $\dot{\bar{\delta}}_x \approx 5 \times 10^{-3}\ \mathrm{s}^{-1}$ while the rate in the y-direction was varied in the range of $\dot{\bar{\delta}}_y \in [0, 2 \times 10^{-2}]\ \mathrm{s}^{-1}$. Figure 16(a) shows the s_x–$\bar{\delta}_x$ responses and Fig. 16(b) the corresponding s_y–$\bar{\delta}_y$ responses. The major problem parameters for this set such as the initiation stresses and the energies absorbed in each direction ($\mathscr{E}_x, \mathscr{E}_y$) and their sum ($\mathscr{E}$) are summarized in Table 2a. The case $\gamma = 0$ represents a confined uniaxial experiment in which $\delta_y = 0$. Here, because of contact of the specimen's sides with the fixed horizontal platens, stress builds up in the y-direction (no s_y–$\bar{\delta}_y$ response for this case). Interestingly, the value of σ_{Ix} is somewhat lower than the value reported in Table 1 for the corresponding pure uniaxial compression test. This is due to the fact that specimens in the pure uniaxial test had a somewhat different cell arrangement than that of the specimens used in the biaxial tests. In the uniaxial test, the specimen had full cells at the four corners as seen in the undeformed configuration in Fig. 7b. By contrast, in the biaxial tests, in an effort to reduce the effect of the corners on the results, the specimens were cut in a way that left no cells at the corners (Fig. 4). Because of the finite size of both specimens, this difference has a small effect on the initiation stress. On the other hand, for the confined test, the energy absorbed at $\bar{\delta}_x = 70\%$ is approximately 3% higher than the value listed in Table 1 which indicates that the effect of this difference in specimen geometry is reduced at higher values of $\bar{\delta}_x$. (The confined uniaxial crushing tests are reminiscent of the work of Stronge and Shim, 1987 who examined the energy absorption capacity of metallic tubes arranged in hexagonal and rectangular arrays crushed dynamically. Detailed results from these tests can be found in Papka, 1998.)

For $\gamma > 0$, the trend in the results is that an extended s_x–$\bar{\delta}_x$ response (in displacement) corresponds

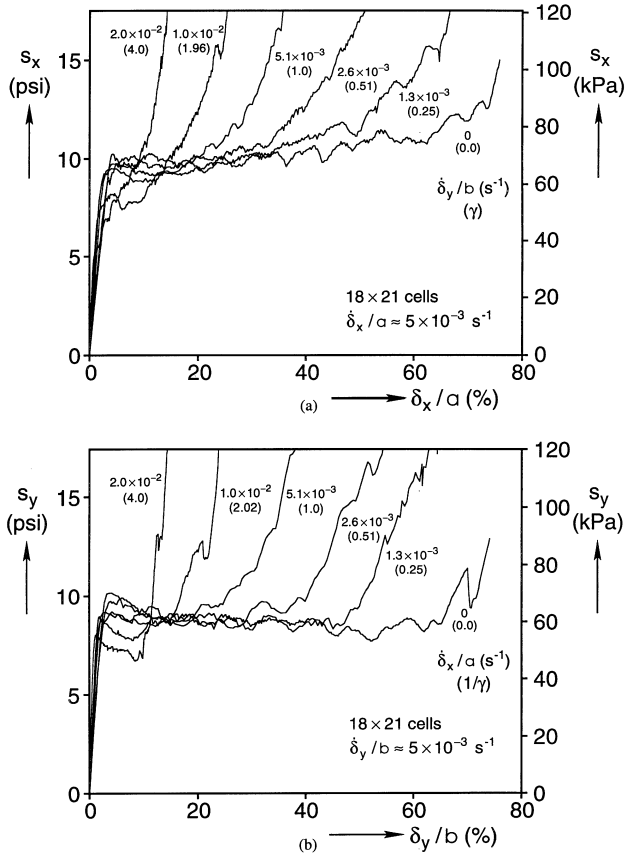

Fig. 16. True stress–displacement responses from the series of tests conducted at various values of γ and $\dot{\bar{\delta}}_x \approx 5\times10^{-3}$ s^{-1}. (a) x-direction and (b) y-direction.

to a shorter s_y–$\bar{\delta}_y$ response and vice versa. All cases exhibit initial load maxima followed by force–displacement responses with negative slopes for part of the loading history. Stiffness is recovered at higher values of net strains in all cases.

Figure 17(a) shows plots of the initiation stresses in the two directions as a function of γ. All values are normalized by the value of σ_{Ix} at $\gamma = 0$. The initiation stress for $\gamma = 0.25$ is approximately 1% higher than the value for $\gamma = 0$. One possible explanation for this is that for $\gamma = 0$, the specimen is only in partial contact with the fixed platens due to initial non-parallelity of the edges of the nearly square specimen. Thus, full confinement does not take place until $\gamma > 0$. For all the values $\gamma > 0$ considered, σ_{Ix} monotonically decreases. By contrast, σ_{Iy} monotonically increases with γ and for $\gamma \sim 4$ attains values corresponding to the higher values of σ_{Ix} recorded.

Figure 18(a) shows plots of the total energy absorbed per unit undeformed volume of the honeycomb ($\mathscr{E}$) as a function of γ. Results are shown for honeycomb volume reductions of 60, 65 and 70%. The three curves traced by the eight experimental points are not parallel, but in all cases, $\mathscr{E}$ starts at a relatively low value for $\gamma = 0$, climbs to a maximum at $\gamma = 1$ and then drops down to the level of the confined uniaxial test. This agrees with the intuitively expected result that a specimen

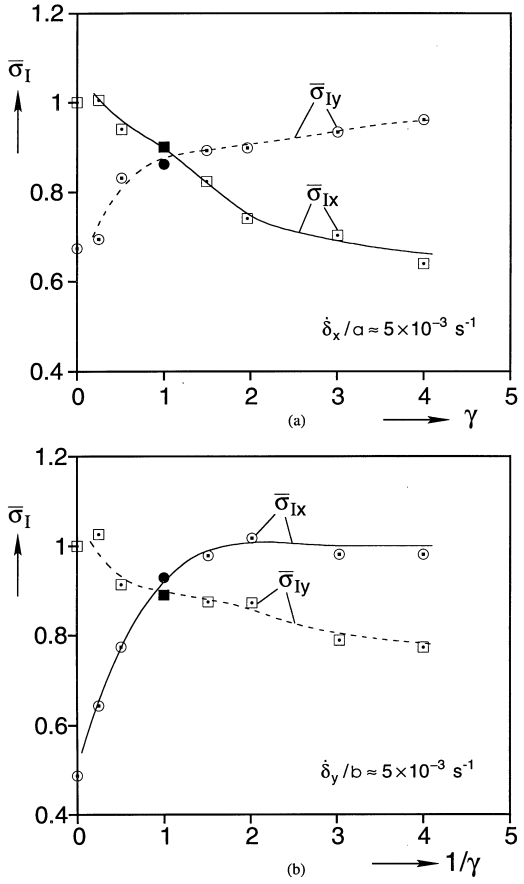

Fig. 17. (a) Initiation stresses in two directions as a function of γ. (b) Initiation stresses in two directions as a function of γ^{-1}.

is harder to deform the more confined it is. Because of its symmetry, the equibiaxial test is the most 'confining' loading imposed and, thus, this test requires the most energy.

Figure 19 shows the true stress–displacement responses from six of the eight experiments in which $\dot{\bar{\delta}}_y \approx 5\times10^{-3}\ \mathrm{s}^{-1}$ while the rate in the x-direction was varied in the range of $\dot{\bar{\delta}}_x \in [0, 2\times10^{-2}]$ s^{-1}. Figure 19(a) shows the s_x–$\bar{\delta}_x$ responses and Fig. 19b the corresponding s_y–$\bar{\delta}_y$ responses. The main parameters of each response are listed in Table 2b. In this set, $\gamma^{-1} = 0$ represents the confined uniaxial test in the y-direction. For this case, the initiation stress, σ_{Iy}, is almost 15% higher than the value measured in the pure uniaxial test listed in Table 1. In addition, the energy absorbed by the time $\bar{\delta}_y = 70\%$ is more than 9% higher than the corresponding value for the pure uniaxial test. Both of these results illustrate the stiffening effect of confinement on the results.

The trend in the responses for $\gamma^{-1} > 0$ is similar to those in Fig. 16, that is, an extended s_y–$\bar{\delta}_y$ response corresponds to a shorter s_x–$\bar{\delta}_x$ response and the reverse. Again, all responses exhibit initial load maxima followed by force–displacement responses with negative slopes. At higher

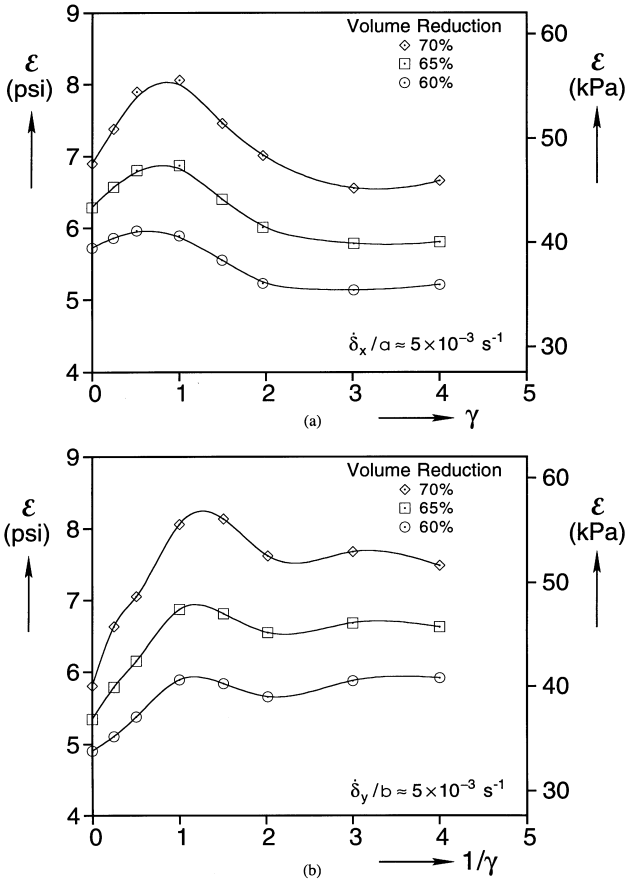

Fig. 18. (a) Energy absorbed during crushing as a function of γ. (b) Energy absorbed during crushing as a function of γ^{-1}.

values of net strains, stiffness is recovered in all cases. The initiation stresses recorded in the two directions, normalized by σ_{Iy} for the confined uniaxial test, are plotted as a function of γ^{-1} in Fig. 17(b). The initiation stress for the confined uniaxial test is somewhat lower than that recorded for $\gamma^{-1} = 0.25$. For $\gamma^{-1} > 0.25$, σ_{Iy} decreases monotonically with γ^{-1} although at a much slower rate than the rate at which σ_{Ix} decreases with γ in Fig. 17(a). At the same time, σ_{Ix} is seen to increase quite significantly between $0 \leqslant \gamma^{-1} < 2$ and subsequently remains relatively unchanged.

The total energy absorbed per unit undeformed volume of the honeycomb is plotted against γ^{-1} in Fig. 18(b). Again, results are shown for honeycomb volume reductions of 60, 65 and 70%. For $\gamma^{-1} < 1$, the energy absorbed increases quite drastically with γ^{-1}. The maximum, once more, corresponds to the equibiaxial case. For $\gamma^{-1} > 2$, $\mathscr{E}$ remains essentially unchanged.

The two plots of $\mathscr{E}$ vs γ and γ^{-1} in Fig. 18, reflect the fact that the uniaxial confined test in the x-direction absorbs 17% more energy than the one in the y-direction (for a volume change of 65%). The maximum value of $\mathscr{E}$ occurs for the equibiaxial test which is common to both plots.

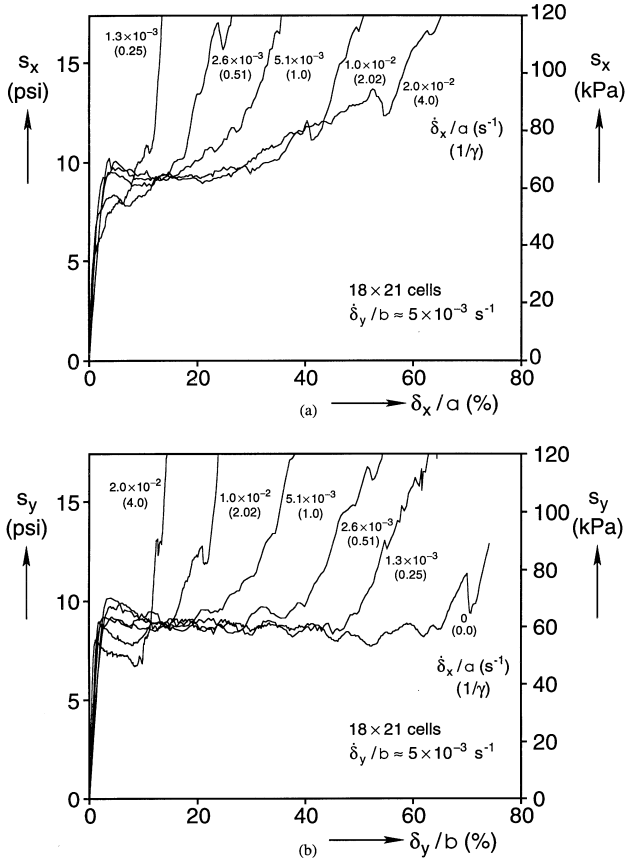

Fig. 19. True stress–displacement responses from the series of tests conducted at various values of γ^{-1} and $\dot{\bar{\delta}}_y \approx 5\times10^{-3}$ s^{-1}. (a) x-direction and (b) y-direction.

Thus, in Fig. 18(a), $\mathscr{E}$ starts at a relatively high value for $\gamma = 0$ and ends at a relatively lower value for $\gamma = 4$. By contrast, in Fig. 18(b), $\mathscr{E}$ starts at a relatively lower value at $\gamma^{-1} = 0$, rises to the maximum at $\gamma^{-1} = 1$ and then approaches the higher value for the confined x-direction uniaxial test at higher values of γ^{-1}.

The effect of rate on the crushing responses was examined in a set of five equibiaxial tests in which the displacement rates of the platens were varied in the range of $\dot{\bar{\delta}} \in [5\times10^{-5}, 5\times10^{-1}]$. The effect of rate on the responses was found to be similar to that reported in Papka and Kyriakides (1998a) for the uniaxial crushing tests in the y-direction. For brevity, we limit attention to the effect of rate on the energy absorbed. Figure 20 shows how the energy absorbed after volume reductions of 60, 65 and 70% changes with the displacement rate. The rate of increase exhibited by $\mathscr{E}$ up to $\dot{\bar{\delta}} \approx 10^{-2}$ is of the same order as the rate at which the propagation stress in Fig. 5 in Papka and Kyriakides (1998a) increases with rate (note that to a first-order $\sigma_{Py} \propto \mathscr{E}_y$). At higher values of $\dot{\bar{\delta}}$, the trend in $\mathscr{E}$ changes. When these higher displacement rate experiments were repeated this trend in $\mathscr{E}$ was found to be persistent. Since all other experimental conditions were the same,

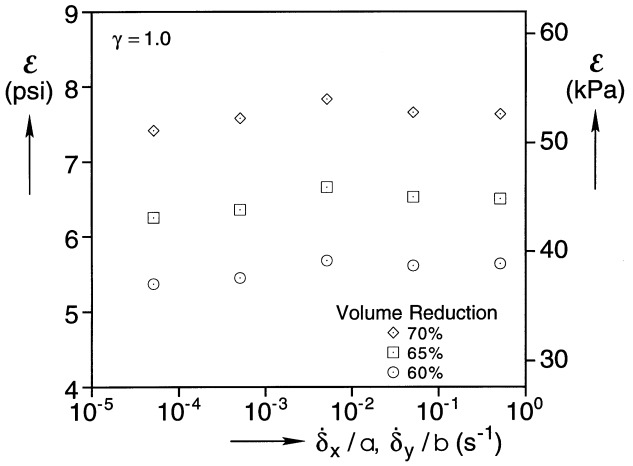

Fig. 20. Energy absorbed in equibiaxial tests conducted at various displacement rates.

we suspect that this change in behavior may be due to changes induced by the higher rate on the stick-slip frictional characteristics of the edges of the specimens and the loading platens. It is important to note that the deformation pattern of Fig. 11 was the prevalent mode of deformation at all rates. Although obviously not exactly the same, no significant difference between the deformed configurations of these five tests was observed.

4. Summary and conclusions

Because of their two-dimensional geometry, honeycombs have been useful as models of the crushing behavior of the broader class of space filling cellular solids. Previously, the authors conducted an extensive study of the crushing behavior of a polycarbonate honeycomb with circular cells under uniaxial compression. The present work examined the crushing of the same honeycomb under biaxial compression. Because of their relatively low density ratios, such materials can be crushed down to very small fractions of their initial volume. To accomplish this under biaxial loading conditions, a new testing facility was developed which utilizes a novel concept of four blocks which slide relative to each other in a way that can result in a volume reduction of the test specimen as high as 95%. The design features and operation of the test facility have been outlined. The test specimen is in contact with orthogonal rigid platens which can be moved either under load or displacement control. By selecting the rate of motion of the platens, the specimen can be crushed to different extents in each direction.

In order to set the stage for the biaxial experiments, results from a uniaxial crushing test in the y-direction (from Papka and Kyriakides, 1998a) were briefly reviewed. For completeness, this was followed by results from a similar experiment crushed in the x-direction. The arrangement of the cells in the two directions is different and, as a result, the modes of localization and the propagation stresses are different. In the y-direction localization develops in a narrow zone affecting a few rows of cells normal to the direction of loading whereas in x-crushing localized collapse is along zones

inclined at $\pm 60^\circ$ to the x-direction. These directions of localization are preferred because of the special alignment of the cells.

The facility was used to conduct a series of biaxial crushing experiments on nearly square honeycomb specimens (18×21 cells). Results from two series of experiments in which the displacement of the platens was prescribed and the biaxiality crushing ratio was varied extensively, have been presented. In each experiment we recorded the true stress–displacement responses in the x- and y-directions as well as full field views of the deformation using a video camera. Three cases with $\gamma = 1$, $\gamma^{-1} = 0.5$ and $\gamma^{-1} = 3$ have been discussed in detail while results from 16 additional experiments have been summarized.

As expected, biaxial crushing is quite complex and the prevalent mechanisms of collapse depend on the biaxiality ratio γ. Localized instabilities are still responsible for the onset of collapse but the extent of localized deformation was found to be more limited than what was observed in the uniaxial crushing tests because of the additional constraints. The various material parameters of interest are influenced to varying degrees by the finite size of the specimens, by friction between the platens and the edges of the honeycomb, by the constraints provided by the rigid platens and, to some degree, by geometric imperfections. Despite these limitations, several interesting cell collapse patterns were identified which depend on γ and γ^{-1}. At higher values of net strains when the net force–displacement responses recover stiffness, the patterns show signs of repeatability in the specimen.

The initial elastic properties and the initiation of instability are influenced the most by the factors mentioned above. This issue will be discussed further in the light of the predictions in Part II. By contrast, the response at larger strains and the energy absorption capacity were found to be much less affected by these factors. Furthermore, despite the fact that the crushing patterns in any two tests were never exactly the same, the responses recorded were quite repeatable.

The energy absorption capacity of the material was found to be the highest under equibiaxial crushing. Its dependence on the rate of crushing was found to follow the same trend as that seen in uniaxial crushing tests in the earlier study.

Acknowledgments

The financial support of the Air Force Office of Scientific Research under Grant No. F49620-98-1-0145 is acknowledged with thanks. The authors wish also to thank Plascore for their cooperation in designing and constructing the honeycomb used in the experiments.

References

Ashby, M.F., 1983. The mechanical properties of cellular solids. Metall. Trans. 14A, 1755–1769.

Gibson, L.J., Ashby, M.F., 1997. Cellular Solids: Structure and Properties 2nd ed. Cambridge University Press, Cambridge, U.K.

Gibson, L.J., Ashby, M.F., Schajer, G.S., Robertson, C.I., 1982. The mechanics of two-dimensional cellular materials. Proc. Royal Society London A382, 25–42.

Klintworth, J.W., Stronge, W.J., 1988. Elasto-plastic yield limits and deformation laws for transversely crushed honeycombs. Int. J. Mechanical Sciences 30, 273–292.

Kyriakides, S., 1994. Propagating instabilities in structures. In: Hutchinson, J.W., Wu, T.Y. (Eds.), Advances in Applied Mechanics, vol. 30. Academic Press Boston, pp. 67–189.

Papka, S.D., 1998. In-plane uniaxial and biaxial crushing of a polycarbonate honeycomb. Ph.D. dissertation, Engineering Mechanics, The University of Texas at Austin.

Papka, S.D., Kyriakides, S., 1994. In-plane compressive response and crushing of honeycomb. J. Mechanics Physics of Solids 42, 1499–1532.

Papka, S.D., Kyriakides, S., 1998a. In-plane crushing of a polycarbonate honeycomb. Int. Journal of Solids and Structures 35, 239–267.

Papka, S.D., Kyriakides, S., 1998b. In-plane crushing of a polycarbonate honeycomb. In: de Borst, R., van der Giessen, E. (Eds.), Material Instabilities in Solids, Proceedings IUTAM Symposium, June 1997, Delft. Wiley, Chichester, U.K., pp. 159–183.

Papka, S.D., Kyriakides, S., 1998c. Experiments and full-scale numerical simulations of in-plane crushing of a honeycomb. Acta Materialia 46 (8), 2765–2776.

Patel, M.R., Finnie, I., 1970. Structural features and mechanical properties of rigid cellular plastics. Journal of Materials 5, 909–932.

Prakash, O., Bichebois, P., Brechet, Y., Louchet, F., Embury, J.D., 1996. A note on the deformation behaviour of two-dimensional model cellular structures. Phil. Magazine A 73, 739–751.

Shaw, M.C., Sata, T., 1966. The plastic behavior of cellular materials. Int. J. Mechanical Sciences 8, 469–478.

Shim, V.P.W., Stronge, W.J., 1986. Lateral crushing of tightly packed arrays of thin-walled metal tubes. Int. J. Mechanical Sciences 28, 709–728.

Triantafyllidis, N., Schraard, M.W., 1998. Onset of failure in honeycomb under general in-plane loading. J. Mechanics Physics Solids 46, 1089–1124.

Warren, W.E., Kraynik, A.M., 1987. Foam mechanics: the linear elastic response of two-dimensional spatially periodic cellular materials. Mechanics of Materials 6, 27–37.

Warren, W.E., Kraynik, A.M., Stone, C.M., 1989. A constitutive model for two-dimensional nonlinear elastic foams. J. Mech. Physics of Solids 37, 717–733.

Zhang, J., Ashby, M.F., 1992. Buckling of honeycombs under in-plane biaxial stresses. Int. J. Mechanical Sciences 34, 491–509.